



Solar photocatalysis for the abatement of emerging micro-contaminants in wastewater: Synthesis, characterization and testing of various TiO₂ samples

Helen Dimitroula^a, Vasileia M. Daskalaki^a, Zacharias Frontistis^a, Dimitris I. Kondarides^b, Paraskevi Panagiotopoulou^b, Nikolaos P. Xekoukoulotakis^a, Dionissios Mantzavinos^{a,*}

^a Department of Environmental Engineering, Technical University of Crete, Polytechnioupolis, GR-73100 Chania, Greece

^b Department of Chemical Engineering, University of Patras, GR-26504 Patras, Greece

ARTICLE INFO

Article history:

Received 10 November 2011

Received in revised form 17 January 2012

Accepted 18 January 2012

Available online 28 January 2012

Keywords:

Characterization

Degradation

Estrogenicity

Kinetics

Preparation

ABSTRACT

The photocatalytic degradation of a mixture of three compounds spiked in secondary treated wastewater by means of simulated solar radiation over titania suspensions was investigated. Bisphenol-A (BPA) and 17 α -ethynylestradiol (EE2) were chosen as representatives of emerging micro-contaminants, while phenol was chosen as a reference contaminant. Ten titania samples were synthesized and employed to evaluate the effect of doping with nitrogen, phosphorous, calcium, silver, sodium and potassium, as well as platinum dispersion on photocatalytic activity. The catalysts were characterized by X-ray diffraction, diffuse reflectance UV–vis spectroscopy, nitrogen physisorption and selective chemisorption of CO or hydrogen.

A 0.5% Pt/TiO₂ catalyst (38 m²/g surface area, 72:28 anatase:rutile, 20 and 2 nm crystallite size for TiO₂ and Pt, respectively) was highly active for the degradation of the contaminants, whose reactivity increased in the order: phenol < BPA \leq EE2; a commercially available Aeroxide P25 TiO₂ exhibited comparable activity.

The effect of various operating conditions, such as 0.5% Pt/TiO₂ concentration (125–1000 mg/L), initial contaminant concentration (100–300 μ g/L each), photon flux (17.4×10^{-8} – 58×10^{-8} einstein/(Ls) provided by a 150 W Xenon lamp) and the water matrix (wastewater and ultrapure water), on degradation was then assessed. Reaction rates increased linearly with catalyst concentration and photon flux, confirming the photo-induced nature of the activation of the catalytic process; likewise, a linear dependence of rate on initial concentration occurred denoting first order kinetics. Degradation in wastewater was slower than in pure water by an order of magnitude, implying the scavenging behavior of effluent's constituents against hydroxyl radicals.

The implications for tertiary wastewater treatment (e.g. mineralization, disinfection and removal of estrogenicity) are also discussed.

© 2012 Elsevier B.V. All rights reserved.

1. Introduction

1.1. The broader context

Heterogeneous photocatalysis based on semiconducting materials and driven by ultraviolet and/or visible light has extensively been researched for the development of several environmental applications including water splitting for hydrogen production, self cleaning surfaces, as well as the decontamination and disinfection of water and air [1]. What could ideally make the process attractive and sustainable would be the use of renewable energy to activate

an inexpensive, stable, readily available and of high quantum yield semiconductor.

As far as the photocatalyst is concerned, the aforementioned requirements are uniquely fulfilled by titania and the fundamentals of TiO₂ photocatalysis can be summarized as follows [2]: the electronic structure of TiO₂, consisting of an empty conduction band and a filled valence band, facilitates the formation of electron–hole pairs when the semiconductor absorbs photonic energy greater than its band gap energy of about 3.2 eV, i.e. at wavelengths below about 390 nm. Holes are strong oxidizing agents and electrons are good reducing agents, therefore both promote redox reactions. Most organic photodegradation reactions utilize the oxidizing power of holes either directly or indirectly, i.e. through the formation of hydroxyl radicals and other reactive oxygen species.

Unfortunately, the wide band gap energy of TiO₂ overlaps only in the UV region of the electromagnetic spectrum; in this view, the

* Corresponding author. Tel.: +30 2821037797; fax: +30 2821037852.

E-mail address: mantzavi@mred.tuc.gr (D. Mantzavinos).

process can utilize only about 6% of the solar energy reaching the earth's surface [3]. This limitation can be overcome modifying titania through e.g. doping with metals and non-metals to narrow the band gap energy and, consequently, enhance photoactivity under visible light [2,3].

1.2. The specific problem

In recent years, there have been intensive efforts toward the development of efficient technologies for the removal of persistent micro-contaminants from aqueous matrices. Discharges of conventional wastewater treatment plants (WWTPs) typically contain a wide array of such compounds at the ng/L–μg/L levels that can only partially be removed by biological and/or adsorption processes [4]. Among others, endocrine disrupting compounds (EDCs) constitute an important class of such contaminants, which pose an increasing threat to aquatic organisms, as well as to human health. EDCs include naturally occurring estrogens, synthetic estrogens, phyto-estrogens and xeno-estrogens (i.e. pesticides, plasticizers, persistent organochlorines, organohalogens, alkyl phenols, heavy metals) [5].

In this work, a mixture of bisphenol-A (BPA), 17α-ethynylestradiol (EE2) and phenol was spiked in secondary wastewater and treated by means of solar photocatalysis in titania suspensions. BPA was chosen as a representative xeno-estrogen typically used in the manufacturing of numerous chemical products, while EE2 is a synthetic estrogen used in the oral contraceptive pill. Both are thought to be associated with endocrine disruption, as well as several other adverse effects [6,7]. Phenol was chosen as a reference compound since it is the precursor of numerous xenobiotics in the environment.

1.3. Research aims

The aim of this work was three-fold:

- (i) To prepare and characterize various TiO₂ samples that could potentially function as effective photocatalysts. Nitrogen and phosphorous were chosen as examples of non-metallic dopant elements that may be used to expand the spectral response of TiO₂ into the visible region of the electromagnetic spectrum by shifting the valence band edge of the semiconductor upwards to narrow its band gap energy [8,9]. Potassium, sodium and calcium were employed as surface promoters that may result in the creation of oxygen vacancies on the TiO₂ surface [10,11] and, therefore, promote adsorption of O₂ and oxidation of organic compounds [12]. Deposition of Pt crystallites on the photocatalyst surface is known to decrease the rate of electron–hole recombination [13], which is one of the key factors that limit overall photocatalytic efficiency. A similar effect is expected for Ag deposits which, depending on

size and shape of Ag nanoclusters, may increase substantially photo-oxidation rates [14].

- (ii) To assess the relative activity of the synthesized catalysts for the degradation of the three contaminants under environmentally realistic conditions, i.e. low concentrations and complex water matrices.
- (iii) To determine key operating parameters that affect degradation kinetics.

Although the degradation of EDCs by TiO₂ photocatalysis has received substantial attention before (recent literature includes references [15–18]), we propose a systematic approach that would help to develop an effective treatment for the abatement of micro-contaminants in waters.

2. Materials and methods

2.1. Contaminants and the water matrix

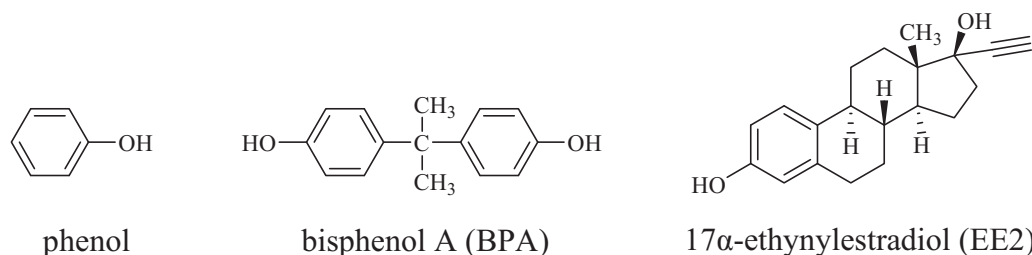
Phenol, BPA and EE2, whose formulae are shown in Scheme 1, were purchased from Sigma–Aldrich and used as received. Stock solutions containing equal concentrations of all three compounds were prepared and the appropriate volume was spiked to the water matrix to achieve the desired concentration in the range 100–300 μg/L for each individual contaminant.

Wastewater (WW) was collected from the outlet of the secondary treatment of the municipal WWTP of Chania, W. Crete, Greece. It was characterized according to standard methods [19] as follows: 24 mg/L chemical oxygen demand, 7.8 mg/L dissolved organic carbon (DOC), 820 μS/cm conductivity and pH 8. Moreover, it contained 220 mg/L chlorides, 188 mg/L bicarbonates, 60 mg/L sulfates, 26 mg/L nitrates and 57 mg/L nitrites, as well as 1200 CFU/mL *Escherichia coli*. Unless otherwise stated, the effluent was first sterilized to inactivate microorganisms and then spiked with the mixture of xenobiotics. This was done to avoid biological degradation of xenobiotics in the stock solutions, as well as for safety reasons.

Some experiments were also performed in ultrapure water (UPW), taken from a water purification system (EASYpureRF – Barnstead/Thermolyne, USA), with 5.5 μS/cm conductivity.

2.2. Synthesis of catalysts

In this work, ten titania catalysts (referred to as samples B–K in Table 1) were synthesized, characterized and tested for the photocatalytic degradation of xenobiotics. Nitrogen-doped TiO₂ was prepared adding slowly 100 mL of aqueous ammonia solution (30%) to 25 mL of Ti(OPr-*i*)₄ (titanium isopropoxide, TIP) at 0 °C under continuous stirring. A white precipitate was formed, which was then filtered in order to remove the solvent. The sample was dried at 110 °C for 24 h and then calcined at 400 °C for 2 h. After calcination a light-yellow powder was obtained.



Scheme 1. Chemical formulae of the contaminants tested in this work.

Table 1

Characterization of the various titania catalysts used in this study.

Catalyst coding	Catalyst type	SSA ^a (m ² /g)	Anatase content ^b (%)	d_{TiO_2} (nm) ^c	Pt dispersion (%)	d_{Pt} ^d (nm)
A	P25 TiO ₂	42	75	23	–	–
B	0.5% Pt/TiO ₂	38	72	20	51	2
C	N-TiO ₂	73	100	13	–	–
D	0.5% Pt/N-TiO ₂	63	100	15	84	1.2
E	P-TiO ₂	175	nd ^e	nd	–	–
F	[H ₃ PO ₄]/[TIP] = 0.1	186	nd	nd	21	4.9
	0.5% Pt/P-TiO ₂					
G	[H ₃ PO ₄]/[TIP] = 0.1	110	nd	nd	–	–
	4% CaO-TiO ₂					
H	[CaO]/[TIP] = 0.05	104	100	7	92	1.1
	0.5% Pt/4%CaO-TiO ₂					
I	[CaO]/[TIP] = 0.05	42	73	23	17	6.2
	0.5% Pt(0.5% Ag)/TiO ₂					
J	0.5% Pt(0.12% Na)/TiO ₂	39	71	22	44	2.3
	0.5% Pt(0.1% K)/TiO ₂					
K	Pt(0.1% K)/TiO ₂	41	71	23	34	3

^a Specific surface area estimated using the BET method.^b TiO₂ phase composition estimated from integral intensities of the anatase (1 0 1) and rutile (1 1 0) XRD reflections.^c Primary crystallite size of TiO₂, estimated from XRD line broadening of the anatase (1 0 1) reflection.^d Mean crystallite size of platinum, estimated from selective chemisorption measurements.^e Not determined.

Phosphorous-doped TiO₂ was prepared employing the following method, which was based on the sol–gel procedure [9]: an aqueous solution (500 mL) of H₃PO₄ was prepared and heated at 90 °C. Then, 50 mL of a 1.2 M clear ethanol solution of TIP was slowly added under continuous stirring. The mixture was refluxed at 90 °C for 4 h, followed by cooling down to room temperature. After filtration, the solid was dried at 90 °C for 24 h and then calcined at 400 °C for 3 h. The molar ratio of [H₃PO₄]/[TIP] was 0.1.

Calcium-promoted TiO₂ was prepared employing the same method used for P-doped catalysts, but adding 4% CaO instead of H₃PO₄. The molar ratio of [CaO]/[TIP] was 0.05.

Dispersed platinum photocatalysts (0.5 wt%) were prepared employing the wet impregnation method with the use of the above carriers and (NH₃)₂Pt(NO₃)₂ (supplied by Alfa) as the platinum precursor salt. All catalysts were reduced at 300 °C in H₂ flow for 2 h. The same method was used for the preparation of Pt catalysts supported on unpromoted TiO₂ carrier. Details on the procedures used for catalyst preparation can be found elsewhere [20].

Alkali- and silver-promoted Pt/TiO₂ catalysts were prepared by co-impregnation of titanium dioxide Aeroxide P25 (formerly known as Degussa P25, supplied by Evonik Industries and referred to as sample A in Table 1) with an aqueous solution containing precursor salts of platinum ((NH₃)₂Pt(NO₃)₂, supplied by Alfa) and the desired promoter (AgNO₃, KNO₃ or NaNO₃). Typically, 3 g of TiO₂ were added under continuous stirring in 50 mL of water containing the desired amount of the salts at inherent solution pH. The resulting slurry was heated slowly at 70 °C under continuous stirring and maintained at that temperature until nearly all the water evaporated. The solid residue was dried at 110 °C for 24 h and then reduced at 300 °C for 2 h in H₂ flow. The nominal Pt loading of all catalysts thus prepared was 0.5 wt%, whereas the promoter concentration was 0.5 wt%, 0.12 wt% and 0.1 wt% for Ag, Na and K, respectively.

2.3. Characterization of catalysts

Catalysts were characterized with respect to their specific surface area (SSA), phase composition and primary crystallite size of the support, and exposed platinum surface area employing nitrogen physisorption at the temperature of liquid nitrogen, X-ray

diffraction (XRD) and selective chemisorption of H₂ or CO, according to the procedures described in detail elsewhere [20]. Diffuse reflectance spectra (DRS) of the synthesized samples were recorded in the range of 200–800 nm at room temperature using a UV–vis spectrophotometer (Varian Cary 3) equipped with an integration sphere.

2.4. Experimental procedure

Photocatalytic experiments were performed using a solar radiation simulator (Newport, model 96000) equipped with a 150 W xenon, ozone-free lamp and an Air Mass 1.5 Global Filter (Newport, model 81094), simulating solar radiation reaching the surface of the earth at a zenith angle of 48.2°.

According to the spectral irradiance data given by the manufacturer (Newport), simulated solar radiation contains about 5% UV-A radiation, and 0.1% UV-B radiation, while the filter cuts radiations with wavelengths lower than 280 nm. The incident photon flux in the photochemical reactor in the UV region of the electromagnetic spectrum was measured actinometrically using 2-nitrobenzaldehyde (purchased from Sigma–Aldrich) as the chemical actinometer [21,22], and it was found to be 58×10^{-8} einstein/(Ls), which corresponds to an irradiance of 13.1×10^{-3} W/m² [21]. To assess the effect of intensity on degradation, suitable filters (FSQ-ND04, 50.8 mm × 50.8 mm, 0.4 optical density and 39.8% transmittance at 633 nm) were employed to reduce the photon flux to 34.8×10^{-8} and 17.4×10^{-8} einstein/(Ls).

Reactions took place in a cylindrical pyrex cell under continuous stirring. Temperature was maintained constant at 25 ± 1 °C with a temperature control unit, while the cell was open to the atmosphere. All runs were performed at the matrix's inherent pH (i.e. about 8 and 6.2 for WW and UPW, respectively), which remained practically unchanged although it was left uncontrolled throughout the reaction. The rationale behind this has to do with the likely repercussions of the proposed treatment that should avoid any unnecessary modifications of the wastewater matrix.

Sixty milliliter of the reaction mixture were introduced in the 150 mL cell, slurried with the appropriate amount of catalyst and left for 20 min in the dark to equilibrate prior to applying solar radiation. For the screening runs described in Section 3.2, catalyst loading was either (i) adjusted accordingly to yield a

common surface area of 1.26 m^2 in the 60 mL reaction mixture (this corresponds to a P25 TiO_2 concentration of 500 mg/L) as in Fig. 3 or (ii) set at 500 mg/L as in Fig. 4. Samples of 0.7 mL were periodically drawn from the reactor, centrifuged at 13,200 rpm to separate the catalyst particles and then analyzed as follows.

2.5. Analytical protocols

High performance liquid chromatography (Alliance 2690, Waters) was employed to monitor the concentration of contaminants. Separation was achieved on a Luna C-18(2) column ($5\text{ }\mu\text{m}$, $250\text{ mm} \times 4.6\text{ mm}$) and a security guard column ($4\text{ mm} \times 3\text{ mm}$), both purchased from Phenomenex. The mobile phase consisting of 35:65 ultrapure water:acetonitrile eluted isocratically at 1 mL/min and 30°C , while the injection volume was $100\text{ }\mu\text{L}$. Detection was achieved through a fluorescence detector (Waters 474 Scanning Fluorescence detector), in which the excitation wavelength was 280 nm and the emission wavelength was 305 nm . The limit of detection was 0.78 , 0.68 and $0.63\text{ }\mu\text{g/L}$ and the limit of quantitation was 2.65 , 2.32 and $2.11\text{ }\mu\text{g/L}$ for phenol, BPA and EE2, respectively.

DOC was measured by non-dispersive infrared gas analysis on a Shimadzu 5050A TOC analyzer.

The yeast estrogen screening (YES) bioassay was employed to assess changes in effluent's estrogenicity according to the protocol originally developed by Routledge and Sumpter [23] with some modifications described by Frontistis et al. [24].

The detection and enumeration of *E. coli* in the effluent were performed using the serial dilution spread plate agar technique as reported in detail elsewhere [25].

3. Results and discussion

3.1. Catalyst properties

The main physicochemical properties of the synthesized catalysts are summarized in Table 1, including SSA, phase composition, primary crystallite size of the doped TiO_2 support (d_{TiO_2}), Pt dispersion and Pt mean crystallite size (d_{Pt}). It is observed that SSA depends strongly on the synthesis method and the nature of the dopant. In particular, SSA is significantly high in the case of phosphorous- and calcium-doped TiO_2 carriers, taking values of $175\text{ m}^2/\text{g}$ and $110\text{ m}^2/\text{g}$, respectively, while the nitrogen-doped TiO_2 carrier is characterized by a lower SSA of $73\text{ m}^2/\text{g}$. The dispersion of Pt on the surface of the above carriers does not change significantly their SSA. The alkali- and silver-promoted Pt/ TiO_2 catalysts are characterized by lower SSAs in the range $39\text{--}42\text{ m}^2/\text{g}$, which are similar to those of the unpromoted Pt/ TiO_2 and P25 TiO_2 catalysts.

X-ray diffraction spectra were obtained for all bare and platinumized catalysts and representative results for calcium-, nitrogen-, alkali- and silver-promoted Pt/ TiO_2 catalysts are shown in Fig. 1. It has been found that nitrogen-, phosphorous- and calcium-doped samples consist of anatase TiO_2 , whereas alkali- and silver-promoted Pt/ TiO_2 catalysts consist of about 72:28 anatase:rutile, i.e. their phase composition is similar to that of the parent material (P25 TiO_2). This is in agreement with previous reports [9,12], which show that introduction of foreign atoms into the crystalline matrix of TiO_2 inhibits the phase transformation of anatase to rutile upon thermal treatment and, as discussed above, also results in materials with high SSA. The primary crystallite size of TiO_2 , determined by XRD peak broadening of the anatase (101) reflection, varies significantly from one sample to another, ranging from 7 nm for $0.5\%\text{Pt}/4\%\text{CaO-TiO}_2$ to 23 nm for $0.5\%\text{Pt}(0.5\%\text{Ag})/\text{TiO}_2$ and $0.5\%\text{Pt}(0.1\%\text{K})/\text{TiO}_2$ catalysts.

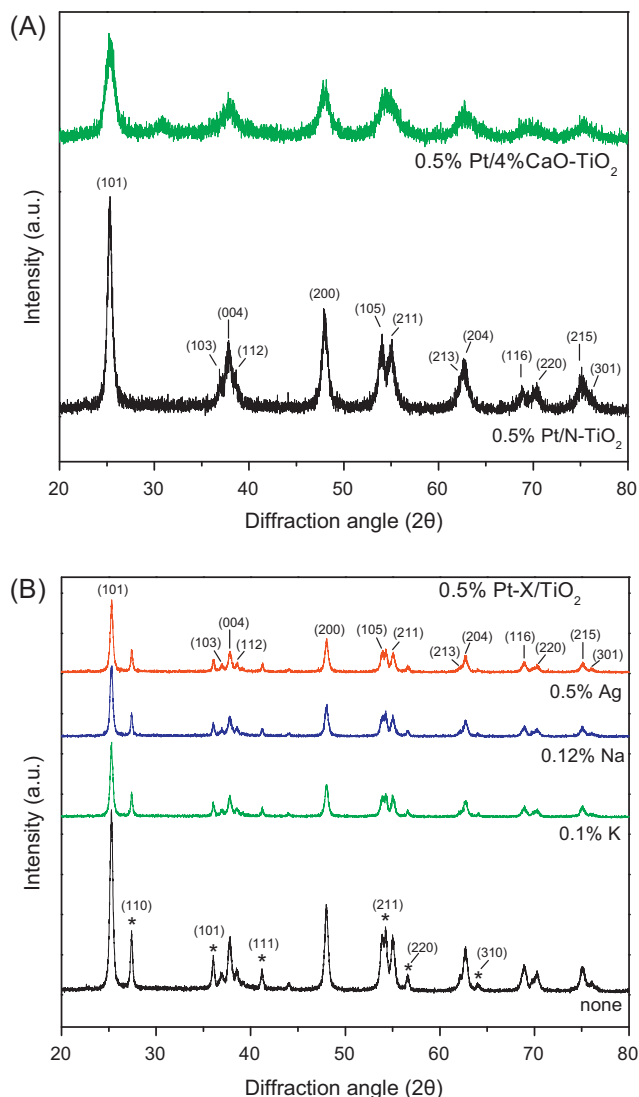


Fig. 1. X-ray diffraction (XRD) spectra of representative titania samples used in this work. Peaks marked with an asterisk correspond to the rutile phase of TiO_2 .

Likewise, the dispersion of Pt and, concomitantly its mean crystallite size (d_{Pt}), vary significantly, taking values between 17% ($d_{\text{Pt}} = 6.2\text{ nm}$) for $0.5\%\text{Pt}(0.5\%\text{Ag})/\text{TiO}_2$ to 92% ($d_{\text{Pt}} = 1.1\text{ nm}$) for $0.5\%\text{Pt}/4\%\text{CaO-TiO}_2$.

Diffuse reflectance spectra of the synthesized samples are shown in Fig. 2. It is observed that titania doping with CaO, P or N results in a shift of the absorbance toward the visible region of the electromagnetic spectrum. The same is also true for the corresponding platinumized samples. These observations are in accordance with results of previous studies focusing on the development of visible light-responsive TiO_2 photocatalysts, which showed that doping of TiO_2 with various kinds of anions [8,9,26,27] or cations [28,29] may lead to a narrowing of the band gap of the semiconductor. In the case of anion-doped TiO_2 , this has been attributed to mixing of the p states of the dopant (e.g., N, P, S, C) with the O2p states of the oxide that shifts the valence band edge upwards, whereas in the case of cation-doped TiO_2 it has been explained by considering that the overlap of the d orbitals of Ti and the d orbitals of the dopant metal ions can introduce new states close to the conduction band [28,30]. It should be noted, however, that shifting the absorption pattern of the semiconductor toward the visible spectral region does not necessarily result in materials with improved photocatalytic performance [30].

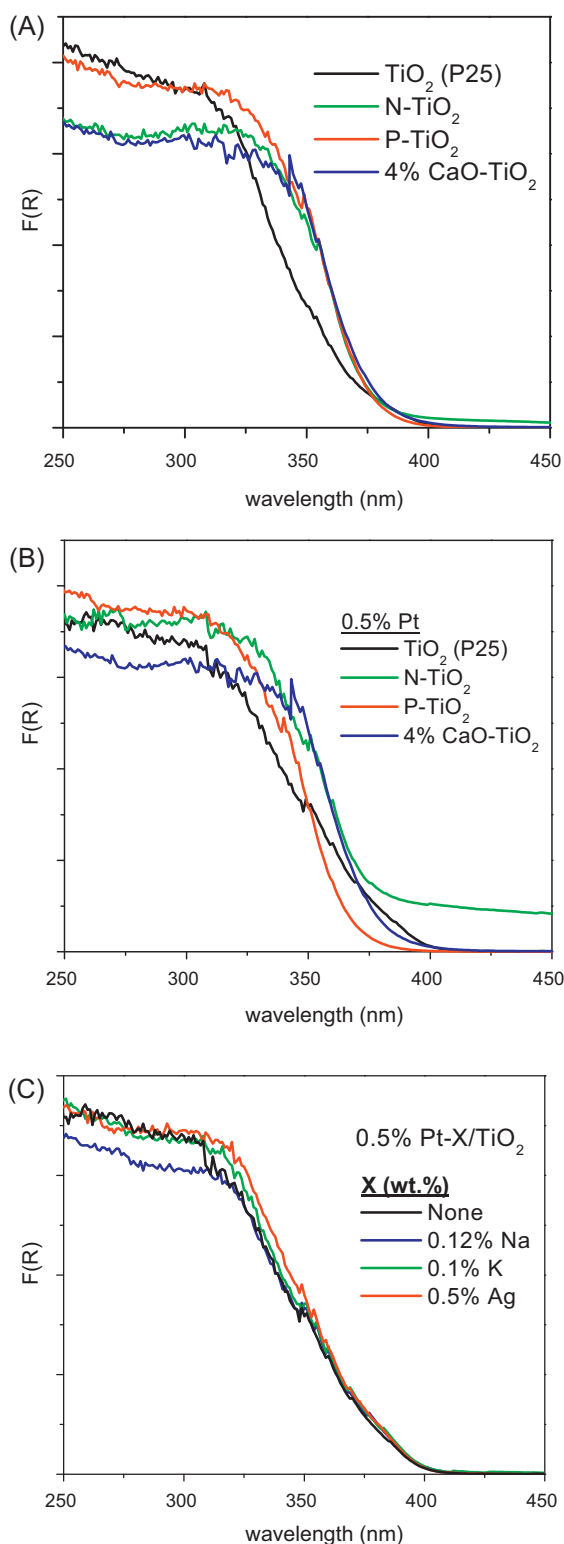


Fig. 2. Diffuse reflectance spectra (DRS) of the titania samples used in this work.

Regarding catalysts promoted with small amounts of alkalis or silver, results presented in Fig. 2 clearly show that addition of these metals does not affect, practically, the absorbance characteristics of TiO_2 . This indicates that the synthesis method employed does not result in incorporation of these dopants into the crystal matrix of the semiconductor. It is known, however, that, because of their strong electropositive character, alkalis may affect the surface

electronic structure as well as the chemisorptive properties and reactivity of TiO_2 [10–12].

3.2. Evaluation of photocatalytic activity

Phenol, BPA and EE2 at 300 $\mu\text{g/L}$ each were spiked to WW and subject to oxidation employing the synthesized catalysts in order to assess their relative activity; runs were performed at a common surface area of 1.26 m^2 in the 60 mL reaction mixture. This was done because photocatalytic reactions mainly occur at or very near the catalyst surface involving the oxidation of adsorbed organics by the locally photogenerated holes, hydroxyl radicals and other reactive oxygen species [2]. In this respect, the surface area itself is critical and would determine kinetics. Although reactions may also occur in the solution phase, their contribution is inferior considering that only a small fraction of the short-lived radicals can survive the migration from the surface to the liquid bulk.

From the respective concentration-time profiles shown in Fig. 3, it is obvious that samples A (P25 TiO_2), B (0.5% Pt/ TiO_2) and J (0.5% Pt(0.12% Na)/ TiO_2) are substantially more active than the rest, yielding at least 90% conversion in 60 min of reaction (with the exception of phenol with sample J, whose conversion is 80%). Bare or platinized samples doped with nitrogen, phosphorous or calcium (C–H) exhibit moderate activity although their absorbance spectra have been shifted toward the visible region (Fig. 2). Similarly, moderate activities are achieved by the silver- and potassium-promoted platinized samples (I and K). Although the addition of silver or potassium appears to be detrimental to the activity of the respective unpromoted sample (B), this is not the case with sodium (J), whose addition does not practically change the activity of sample B. Regardless of the catalyst employed, the contaminant reactivity increases in the order: phenol < BPA \leq EE2. To confirm that degradation is due to the synergy between photonic energy and the catalyst, an additional experiment was performed in the absence of catalyst, yielding just 6% conversion after 60 min for either contaminant (data not shown for brevity).

It should be noted that treatment efficiency and, consequently, relative catalytic activity may strongly depend on the operating conditions in question, such as the catalyst to contaminant concentration ratio and the water matrix (their effects will be discussed in Sections 3.3 and 3.4), as well as on the criteria according to which efficiency is assessed. Table 2 compares samples A, B and J in terms of initial (i.e. after 5 min) degradation rates and the time needed to achieve 90% contaminant degradation. Since samples B and J were reduced at 300 $^\circ\text{C}$ during preparation, an additional run was performed with sample A being pretreated at the same temperature (denoted as sample A*) and the respective results are also given in Table 2. As seen, the two platinized catalysts are slightly more active than bare TiO_2 for BPA and EE2 degradation, while the opposite is true for phenol; moreover, thermal treatment of P25 TiO_2 appears to have a detrimental effect on its photocatalytic performance.

When platinum is deposited onto the titania surface, a Schottky barrier is formed and the metal serves as an electron sink. This results in a more efficient separation of holes from electrons since their recombination is a major cause for reduced photocatalytic activity [31]. Chiang et al. [32], who studied the photocatalytic degradation of 20 mg/L BPA under UV-A radiation, reported that the degradation rate of BPA increased by 1.4 and 3.2 times when bare P25 TiO_2 was added 0.2% and 1% Pt, respectively. Experiments with EE2 and BPA at the low mg/L level (i.e. 0.8–2.3 mg/L) gave similar degradation rates for bare and platinized P25 TiO_2 under UV-A radiation [31]; nevertheless, when the experiments were repeated at higher contaminant concentrations (i.e. 40 mg/L), a 2% Pt/ TiO_2 catalyst was more effective than its bare counterpart. The authors [31] argued that at relatively low contaminant levels,

Table 2
Comparison of various titania catalysts for the photocatalytic degradation of phenol, BPA and EE2 in wastewater. Other conditions as in Fig. 3 Catalyst coding as in Table 1.

Compound	Initial rate ($\mu\text{g}/(\text{L min})$) ^a				Time for 90% conversion (min)			
	A	B	J	A ^{*b}	A	B	J	A ^{*b}
Phenol	9.8	4.6	4.1	5.4	50–60	60	>75	90
BPA	13.5	20.9	19.8	14.4	40	30–40	30–40	60
EE2	18.5	21.2	21.2	16.1	40–50	30	30	60

^a After 5 min of reaction.

^b A^{*} corresponds to P25 TiO₂ pretreated at 300 °C.

the concentration of oxidizing species generated by P25 TiO₂ (whose well-documented activity is usually ascribed to the low electron–hole recombination rate [33]) was in excess, thus masking the beneficial effect of platinum; this effect though became more

pronounced at higher contaminant to oxidizing species concentration ratio.

Since catalyst photoactivation is associated with the number of particles that are exposed to illumination and given that catalyst

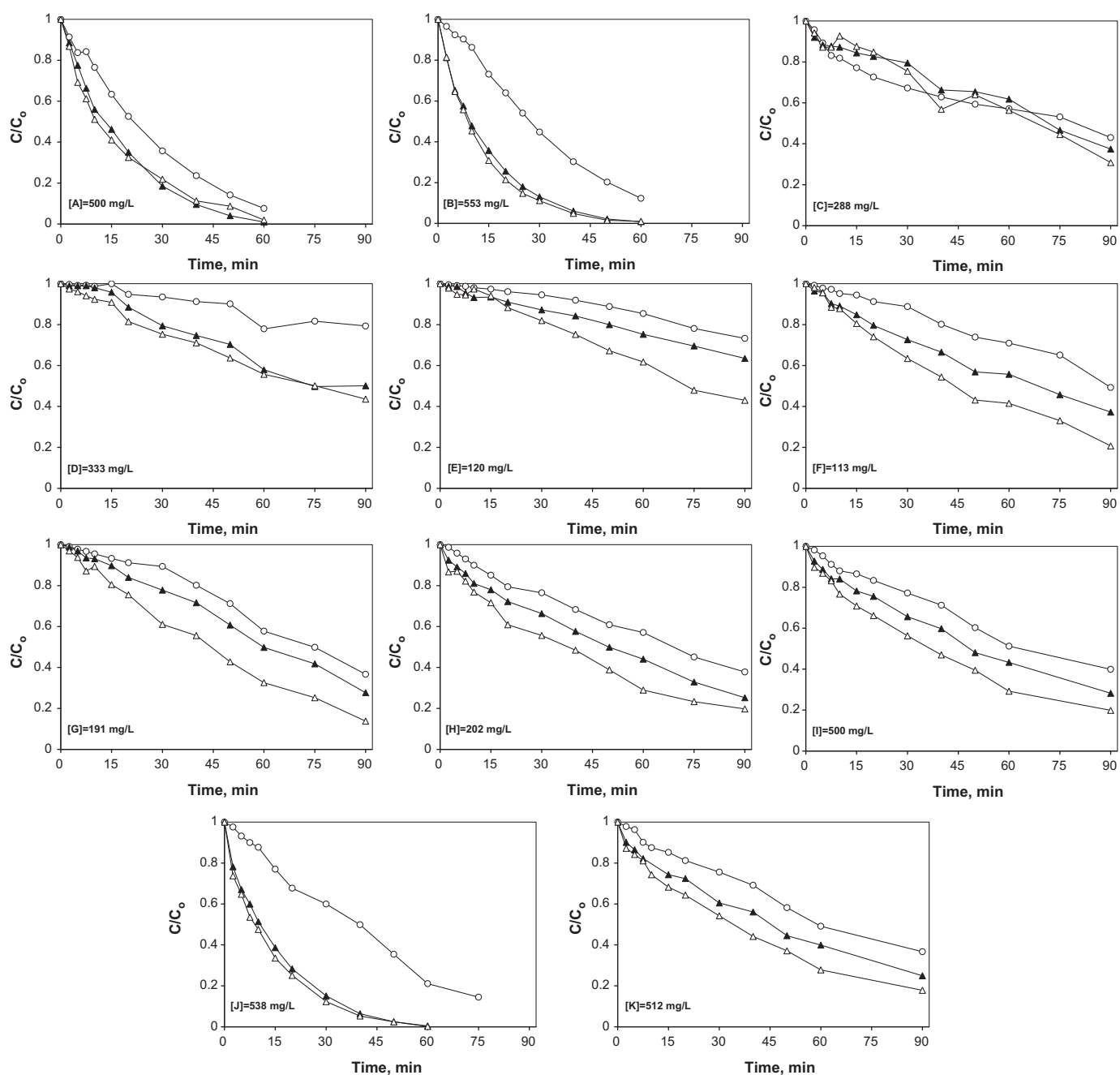


Fig. 3. Relative photocatalytic activity of various titania samples for the degradation of phenol (○), BPA (▲) and EE2 (△) in wastewater. [Phenol]₀ = [BPA]₀ = [EE2]₀ = 300 $\mu\text{g}/\text{L}$; 58×10^{-8} einstein/(L s) of photon flux. Catalyst coding as in Table 1.

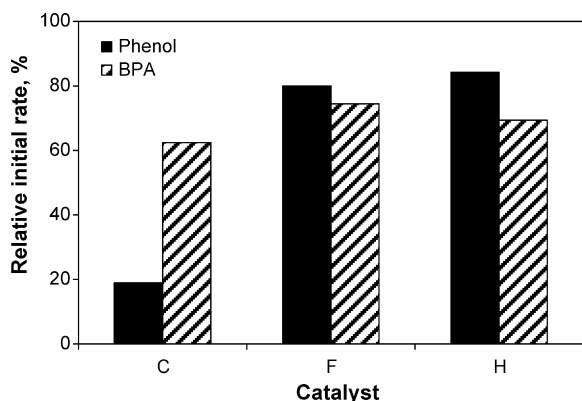


Fig. 4. Relative initial rate of BPA and phenol degradation in wastewater at 500 mg/L catalyst loading. $[\text{Phenol}]_0 = [\text{BPA}]_0 = [\text{EE2}]_0 = 300 \mu\text{g/L}$. Photon flux = 58×10^{-8} einstein/(L s).

loading may affect the extent of light penetration in the reactor and/or its scattering [2], one may argue that relative activity should have been evaluated on the basis of a common mass rather than surface area. In this view, a series of experiments were performed with samples A (P25 TiO_2), C (N- TiO_2), F (0.5% Pt/P- TiO_2) and H (0.5% Pt/4%CaO- TiO_2) at a common catalyst loading of 500 mg/L. Samples C, F and H were selected because they have substantially greater SSAs and different structures than sample A (and B or J, indeed). Fig. 4 shows initial degradation rates with samples C, F or H relative to the rate with sample A; as clearly seen, P25 TiO_2 is still more active than the rest although the available surface area for reactions is up to 4.5 times less.

3.3. Effect of catalyst loading

The effect of 0.5% Pt/ TiO_2 loading on the degradation of phenol, BPA and EE2 was studied in the range 125–1000 mg/L and representative concentration-time profiles for BPA are shown in Fig. 5 (phenol and EE2 profiles exhibit similar trends and, therefore, they are not shown for the sake of brevity). Degradation is favored at higher catalyst loadings, e.g. 90% BPA conversion can be achieved after 25 min at 1000 mg/L or 50 min at 125 mg/L catalyst. The inset of Fig. 5 shows a linear dependence of initial reaction rate, r_0 , on catalyst loading for either contaminant and this is characteristic of a heterogeneous catalytic regime [34]. Increasing catalyst loading apparently results in an increased number of catalyst active sites

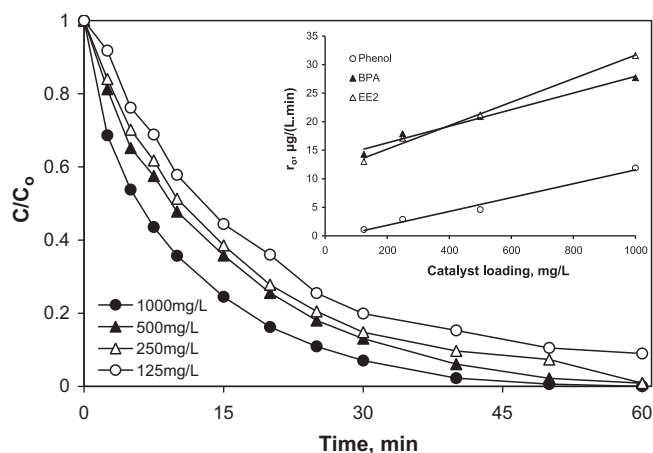


Fig. 5. Effect of 0.5% Pt/ TiO_2 loading on the photocatalytic degradation of BPA in wastewater. Inset graph: dependence of initial rate on 0.5% Pt/ TiO_2 loading. $[\text{Phenol}]_0 = [\text{BPA}]_0 = [\text{EE2}]_0 = 300 \mu\text{g/L}$. Photon flux = 58×10^{-8} einstein/(L s).

that are available for photocatalytic reactions and this occurs up to a point where all catalyst particles become fully illuminated [35].

3.4. Effects of initial contaminant concentration and the water matrix

Fig. 6 shows the effect of varying initial contaminant concentration on degradation. With the exception of phenol at the highest concentration of 300 $\mu\text{g/L}$, complete contaminant degradation can be achieved at reaction times no longer than 60 min. Initial rates, summarized in Table 3, appear to increase nearly linearly with contaminant concentration, C , which is characteristic of first order kinetics with respect to C , i.e.:

$$r = -\frac{dC}{dt} = kC[\text{Ox}]^n = k_{\text{app}}C \Leftrightarrow \ln \frac{C_0}{C} = k_{\text{app}}t \quad (1)$$

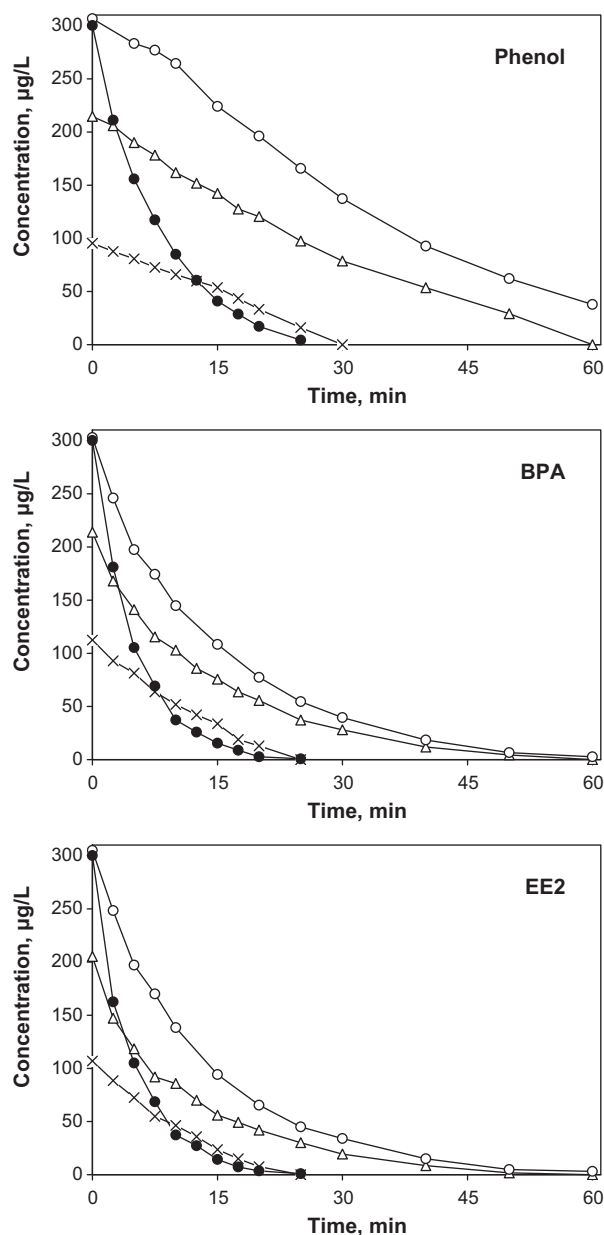


Fig. 6. Effect of initial contaminant concentration and water matrix on the photocatalytic degradation. (○) 300 $\mu\text{g/L}$ in WW; (●) 300 $\mu\text{g/L}$ in UPW; (△) 200 $\mu\text{g/L}$ in WW; (×) 100 $\mu\text{g/L}$ in WW. [0.5% Pt/ TiO_2] = 500 mg/L; 58×10^{-8} einstein/(L s) of photon flux.

Table 3
Effect of initial contaminant concentration and photon flux on the initial degradation rate (calculated after 5 min in $\mu\text{g}/(\text{L}\cdot\text{min})$) of phenol, BPA and EE2 in wastewater. $[0.5\% \text{ Pt}/\text{TiO}_2] = 500 \text{ mg/L}$.

Conditions	Phenol	BPA	EE2
$[\text{Phenol}]_0 = [\text{BPA}]_0 = [\text{EE2}]_0 = 100 \mu\text{g/L}$, $58 \times 10^{-8} \text{ einstein}/(\text{L}\cdot\text{s})$	2.9	6.2	6.9
$[\text{Phenol}]_0 = [\text{BPA}]_0 = [\text{EE2}]_0 = 200 \mu\text{g/L}$, $58 \times 10^{-8} \text{ einstein}/(\text{L}\cdot\text{s})$	4.9	14.5	17.3
$[\text{Phenol}]_0 = [\text{BPA}]_0 = [\text{EE2}]_0 = 300 \mu\text{g/L}$, $58 \times 10^{-8} \text{ einstein}/(\text{L}\cdot\text{s})$	4.6	20.9	21.2
$[\text{Phenol}]_0 = [\text{BPA}]_0 = [\text{EE2}]_0 = 300 \mu\text{g/L}$, $34.8 \times 10^{-8} \text{ einstein}/(\text{L}\cdot\text{s})$	3.9	16	18.2
$[\text{Phenol}]_0 = [\text{BPA}]_0 = [\text{EE2}]_0 = 300 \mu\text{g/L}$, $17.4 \times 10^{-8} \text{ einstein}/(\text{L}\cdot\text{s})$	0	11.1	14.4

where k is the reaction rate constant, k_{app} is an apparent, first order, rate constant $[\text{Ox}]$ is the concentration of oxidizing species and n is the reaction order regarding $[\text{Ox}]$.

The ability of semiconductor photocatalysts to oxidize organic species is due to the valence band holes photogenerated onto the titania surface, as well as the hydroxyl radicals, HO^\bullet , produced from the reaction of holes with surface-bound water and hydroxyl anions. Moreover, the formation of perhydroxyl radicals, HO_2^\bullet , through reactions involving photogenerated conduction band electrons, dissolved oxygen and protons cannot be excluded [36,37]. Hydroxyl radicals are considered as the primary oxidizing agent acting not only on the surface but also in the solution phase [36]. The collective concentration of all possible oxidizing species in the reaction mixture should be constant at fixed operating conditions since their generation rate should only depend on the photon flux and the catalyst loading; in this respect, the term $[\text{Ox}]^n$ can be incorporated to k_{app} . An increase in contaminant concentration would increase the probability of $[\text{Ox}]$ attack and, consequently, the reaction rate. This increase is almost linear for the range of concentrations in question, denoting first order kinetics. If experiments were performed at higher concentrations $[\text{Ox}]$ would become the limiting reactant and, consequently, a transition to lower order kinetics would most probably occur.

The experiment at the highest contaminant concentration was also performed in UPW in an attempt to evaluate the effect of water matrix on photocatalytic performance; from the respective profiles shown in Fig. 6, it is obvious that reactions in UPW occur much faster than in WW, e.g. complete degradation can be achieved in 20–25 min for either contaminant. If the results of Fig. 6 at $300 \mu\text{g/L}$ concentration and up to 90% conversion for each contaminant are plotted in the form of Eq. (1), straight lines passing through the origin fit the data very well (i.e. the coefficient of linear regression, r^2 , is typically greater than 99%). From the slopes of the resulting straight lines (not shown), the computed k_{app} values in WW are 30.8×10^{-3} , 68.8×10^{-3} and $75.7 \times 10^{-3} \text{ min}^{-1}$ for phenol, BPA and EE2, respectively, while the corresponding values in UPW are 13.1×10^{-2} , 20×10^{-2} and $19.9 \times 10^{-2} \text{ min}^{-1}$, i.e. an order of magnitude greater.

The detrimental impact of water matrix on kinetics is associated with the organic and inorganic species inherently present in the wastewater that compete with the spiked contaminants for hydroxyl radicals and other oxidizing agents. We have recently shown that the effluent organic matter (EfOM), which typically consists of biomass-associated products (e.g. polysaccharides) and humic-type substances, is highly resistant to advanced oxidation by homogeneous solar Fenton oxidation [38], UV-A/ TiO_2 photocatalysis [39] and anodic oxidation [40]. At the conditions of Fig. 6, EfOM, whose concentration is 11 times greater than that of the three contaminants together, is highly resistant to mineralization (see also Section 3.6); therefore, it is reasonable to assume that oxidizing species are partly consumed in reactions involving EfOM. Furthermore, hydroxyl radicals may be scavenged by bicarbonates, chlorides and sulfates present in wastewater to form the respective radicals, whose oxidation potential is lower than that of hydroxyl

radicals [41,42]. Yap and Lim [43], who studied the solar photocatalytic degradation of BPA in N-doped TiO_2 , reported that the addition of inorganic ions such as chlorides, bicarbonates and sulfates in UPW reduced kinetics and so did the presence of methanol competing with BPA for oxidizing species, as well as catalyst active sites.

3.5. Effect of photon flux

Fig. 7 shows the concentration-time profiles of phenol, BPA and EE2 during photocatalytic degradation at photon flux values of 34.8×10^{-8} and $17.4 \times 10^{-8} \text{ einstein}/(\text{L}\cdot\text{s})$. From Figs. 6 and 7, one can clearly see that contaminant degradation decreases with decreasing photon flux, e.g. the 60-min phenol conversion is 87.4%, 59.5% and 31.8% at 58×10^{-8} , 34.8×10^{-8} and $17.4 \times 10^{-8} \text{ einstein}/(\text{L}\cdot\text{s})$, respectively. Table 3 summarizes initial rates as a function of photon flux showing a linear dependence for BPA and EE2. These findings verify the light-driven nature of the activation of the catalytic process, involving the participation of photogenerated holes and electrons [34]. At relatively low fluxes (as those employed in this study), the holes, whose concentration is considerably lower than that of photogenerated and n-type electrons, are produced proportionately to the photon flux and depleted to (i) oxidize the contaminants either directly or through the formation of hydroxyl radicals, and (ii) recombine with electrons. In this case, oxidation reactions dominate over recombination and, therefore, their rate is proportional to the photon flux [2]. At higher fluxes though, the concentration of holes increases substantially and this also increases the possibility of electron–hole recombination, thus reducing the quantum yield; in this case, the reaction rate appears to be proportional to the square root of flux [2]. It should be noted that the exact value of flux, at which such transition would occur

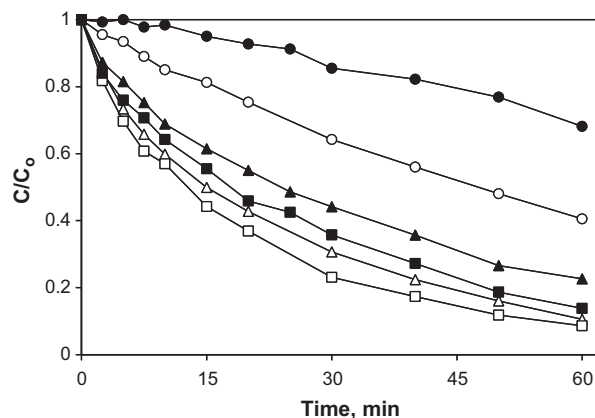


Fig. 7. Effect of photon flux on the photocatalytic degradation of phenol (\circ , \bullet), BPA (\triangle , \blacktriangle) and EE2 (\square , \blacksquare) in wastewater. Open and filled symbols refer to 34.8×10^{-8} and $17.4 \times 10^{-8} \text{ einstein}/(\text{L}\cdot\text{s})$, respectively. $[\text{Phenol}]_0 = [\text{BPA}]_0 = [\text{EE2}]_0 = 300 \mu\text{g/L}$; $[0.5\% \text{ Pt}/\text{TiO}_2] = 500 \text{ mg/L}$.

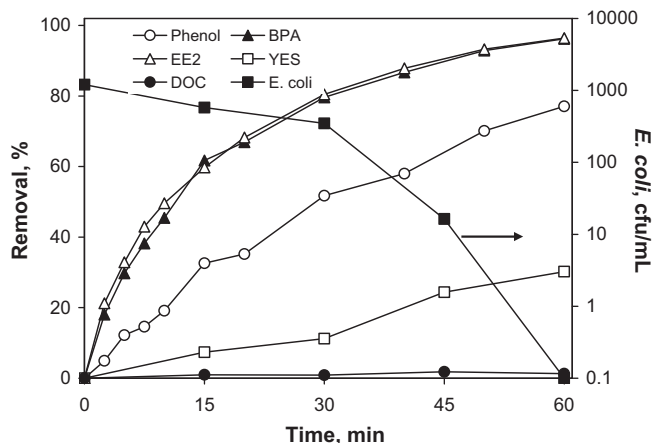


Fig. 8. Efficiency of solar photocatalysis for tertiary wastewater treatment. $[\text{Phenol}]_0 = [\text{BPA}]_0 = [\text{EE2}]_0 = 300 \mu\text{g/L}$; $[\text{E. coli}]_0 = 1200 \text{ CFU/mL}$; $[0.5\% \text{ Pt/TiO}_2] = 500 \text{ mg/L}$; $58 \times 10^{-8} \text{ einstein/(Ls)}$ of photon flux.

depends on the specific experimental conditions but a typical value would be in the order of 20 W/m^2 [2].

3.6. Implications for tertiary treatment

A final experiment was performed to assess process efficiency for tertiary treatment and, in this case, the water matrix had not been sterilized before. As seen in Fig. 8, the proposed process is capable of decomposing the individual contaminants in question, as well as inactivating pathogens but it cannot mineralize the effluent. This seems to be consistent with the relatively low removal of overall estrogenicity (e.g. 30% after 60 min) which may be due to: (i) the formation of partial oxidation, estrogenic by-products from phenol, BPA and EE2, (ii) unreacted phenol (i.e. 23% after 60 min), and (iii) the likely interactions among intrinsically estrogenic EfOM fractions, the spiked contaminants and their oxidation by-products.

It should be noted that the effluent's inherent estrogenicity was $7 \mu\text{g/L}$ equivalent, which increased to $258 \mu\text{g/L}$ after spiking. Given that the estrogenicity of the spiked matrix is far greater than that of the actual effluent (due to the unrealistically high concentration of spiked contaminants at $900 \mu\text{g/L}$), one may expect a more effective estrogenicity removal at lower, more realistic concentrations. It is evident from these results though that the estrogenicity induced by specific compounds is not fully eliminated upon their removal.

4. Conclusions

The fate of emerging micro-contaminants in environmentally relevant samples has attracted considerable attention over the past few years. Semiconductor photocatalysis based on TiO_2 and driven by solar radiation may offer a conceptually advantageous, sustainable technology to treat such contaminants. The major conclusions drawn from this study are summarized as follows:

- (1) Modification of titania through doping with metals and non-metals to enhance photoactivity under visible light was attempted but it did not improve treatment performance. Conversely, dispersion of platinum in bare Aeroxide P25 TiO_2 enhanced activity and this is thought to be associated with a more efficient separation of photogenerated holes from electrons.
- (2) Degradation is affected by operating parameters like catalyst loading, initial contaminant concentration and photon flux. At the conditions in question, the dependence of the reaction rate on these parameters was found to be linear.

- (3) Degradation in pure water was an order of magnitude faster than in secondary treated effluent, thus implying the key role of the water matrix. This pinpoints the need to (i) work with actual environmental samples rather than model or synthetic solutions, and (ii) define treatment objectives that can go beyond the removal of individual contaminants to include disinfection and mineralization.

Acknowledgments

The authors wish to thank Dr D. Fatta-Kassinos (University of Cyprus) and Dr E. Routledge (Brunel University, UK) for supplying yeasts for the YES test.

References

- [1] C. McCullagh, N. Skillen, M. Adams, P.K.J. Robertson, J. Chem. Technol. Biotechnol. 86 (2011) 1002–1017.
- [2] S. Malato, P. Fernandez-Ibanez, M.I. Maldonado, J. Blanco, W. Gernjak, Catal. Today 147 (2009) 1–59.
- [3] M.D. Hernandez-Alonso, F. Fresno, S. Suarez, J.M. Coronado, Energy Environ. Sci. 2 (2009) 1231–1257.
- [4] M. Klavarioti, D. Mantzavinos, D. Kassinos, Environ. Int. 35 (2009) 402–417.
- [5] M. Aurio, Y. Filali-Meknassi, R.D. Tyagi, C.D. Adams, R.Y. Surampalli, Process Biochem. 41 (2006) 525–539.
- [6] J.H. Kang, D. Aasi, Y. Katayama, Crit. Rev. Toxicol. 37 (2007) 607–625.
- [7] E.J. Routledge, D. Sheahan, C. Desbrow, G.C. Brighty, M. Waldock, J.P. Sumpter, Environ. Sci. Technol. 32 (1998) 1559–1565.
- [8] R. Asahi, T. Morikawa, T. Ohwaki, K. Aoki, Y. Taga, Science 293 (2001) 269–271.
- [9] H.-F. Yu, J. Phys. Chem. Solids 68 (2007) 600–607.
- [10] P. Panagiotopoulou, D.I. Kondarides, J. Catal. 267 (2009) 57–66.
- [11] P. Panagiotopoulou, D.I. Kondarides, Appl. Catal. B 101 (2011) 738–746.
- [12] S.G. Kumar, L.G. Devi, J. Phys. Chem. A 115 (2011) 13211–13241.
- [13] A.L. Linsebigler, G. Lu, J.T. Yates Jr., Chem. Rev. 95 (1995) 735–758.
- [14] P. Christopher, D.B. Ingram, S. Linic, J. Phys. Chem. C 114 (2010) 9173–9177.
- [15] M.J. Benotti, B.D. Stanford, E.C. Wert, S.A. Snyder, Water Res. 43 (2009) 1513–1522.
- [16] G. Li Puma, V. Puddu, H.K. Tsang, A. Gora, B. Toepfer, Appl. Catal. B 99 (2010) 388–397.
- [17] D.P. Subagio, M. Srinivasan, M. Lim, T.-T. Lim, Appl. Catal. B 95 (2010) 414–422.
- [18] X. Wang, T.-T. Lim, Appl. Catal. B 100 (2010) 355–364.
- [19] L.S. Clesceri, A.E. Greenberg, A.D. Eaton, Standard Methods for the Examination of Water and Wastewater, twentieth ed., APHA, 1999.
- [20] P. Panagiotopoulou, D.I. Kondarides, J. Catal. 225 (2004) 327–336.
- [21] K.L. Willett, R.A. Hites, J. Chem. Educ. 77 (2000) 900–902.
- [22] E.S. Galbavy, K. Ram, C. Anastasio, J. Photochem. Photobiol. A 209 (2010) 186–192.
- [23] E.J. Routledge, J.P. Sumpter, Environ. Toxicol. Chem. 15 (1996) 241–248.
- [24] Z. Frontistis, V.M. Daskalaki, A. Katsaounis, I. Poulis, D. Mantzavinos, Water Res. 45 (2011) 2996–3004.
- [25] E. Chatzisympson, A. Droumpali, D. Mantzavinos, D. Venieri, Photochem. Photobiol. Sci. 10 (2011) 389–395.
- [26] S.U.M. Khan, M. Al-Shahry, W.B. Ingler Jr., Science 297 (2002) 2243–2245.
- [27] T. Umebayashi, T. Yamaki, H. Itoh, K. Asai, Appl. Phys. Lett. 81 (2002) 454–456.
- [28] M. Anpo, M. Takeuchi, J. Catal. 216 (2003) 505–515.
- [29] W. Choi, A. Termin, M.R. Hoffmann, J. Phys. Chem. 98 (1994) 13669–13679.
- [30] M.A. Henderson, Surf. Sci. Rep. 66 (2011) 185–297.
- [31] H.M. Coleman, K. Chiang, R. Amal, Chem. Eng. J. 113 (2005) 65–72.
- [32] K. Chiang, T.M. Lim, L. Tsen, C. Chow Lee, Appl. Catal. A 261 (2004) 225–237.
- [33] C.A. Emilio, M.I. Litter, K. Marinus, M. Bouchard, C. Colbeau-Justin, Langmuir 22 (2006) 3606–3613.
- [34] J.-M. Herrmann, Appl. Catal. B 99 (2010) 461–468.
- [35] L. Yang, L.E. Yu, M.B. Ray, Water Res. 42 (2008) 3480–3488.
- [36] C.S. Turchi, D.F. Ollis, J. Catal. 122 (1990) 178–192.
- [37] M.R. Hoffman, S. Martin, W. Choi, D. Bahnemann, Chem. Rev. 95 (1995) 69–96.
- [38] Z. Frontistis, N.P. Xekoukoulakis, E. Hapeshi, D. Venieri, D. Fatta-Kassinos, D. Mantzavinos, Chem. Eng. J. 178 (2011) 175–182.
- [39] E. Dialynas, D. Mantzavinos, E. Diamadopoulos, Water Res. 42 (2008) 4603–4608.
- [40] Z. Frontistis, C. Brebou, D. Venieri, D. Mantzavinos, A. Katsaounis, J. Chem. Technol. Biotechnol. 86 (2011) 1233–1236.
- [41] M. Chihai, O. Hamdaoui, S. Baup, N. Gondrexon, Ultrason. Sonochem. 18 (2011) 943–950.
- [42] I. Poulis, G. Kyriacou, Environ. Technol. 23 (2002) 179–187.
- [43] P.-S. Yap, T.-T. Lim, Appl. Catal. B 101 (2011) 709–717.